Research Article Vol. 30, No. 26 / 19 Dec 2022 / Optics Express 48051
Optics EXPRESS

On-chip integrated quantum emitter with 'trap-enhance-guide': a simulation approach

SAMPRITY SAHA,[1] CHUCHUAN HONG,[2] DHRUV FOMRA,[1] UMIT OZGUR,[1] VITALY AVRUTIN,[1] JUSTUS C. NDUKAIFE,[2,3] AND NATHANIEL KINSEY[1,*]

[1]*Department of Electrical and Computer Engineering, Virginia Commonwealth University, Richmond, VA 23220, USA*
[2]*Department of Electrical and Computer Engineering, Vanderbilt University, Nashville, TN 37235, USA*
[3]*justus.ndukaife@vanderbilt.edu*
[*]*nkinsey@vcu.edu*

Abstract: To address the challenges of developing a scalable system of an on-chip integrated quantum emitter, we propose to leverage the loss in our hybrid plasmonic-photonic structure to simultaneously achieve Purcell enhancement as well as on-chip maneuvering of nanoscale emitter via optical trapping with guided excitation-emission routes. In this report, we have analyzed the feasibility of the functional goals of our proposed system in the metric of trapping strength (~8K_BT), Purcell factor (>1000~), and collection efficiency (~10%). Once realized, the scopes of the proposed device can be advanced to develop a scalable platform for integrated quantum technology.

1. Introduction

Over the recent years there has been increasing interest to implement quantum technologies with integrated photonic networks which are prerequisites of an on-chip, scalable system of quantum emitters with enhanced carrier decay rate [1]. There has been extraordinary progress on achieving large enhancement of nano emitters by analyzing plasmonic nanostructures for efficient coupling and light-matter interaction [2–4]. While coupling extrinsic emitters to plasmonic structures adds flexibility in the design of the system, it also requires precise positioning of the nanodots to access the critically small plasmonic mode volume supporting large Purcell enhancement [5,6]. The traditional approaches of emitter placement near plasmonic nanoantenna in prior seminal works typically involved either probabilistic drop-casting [2,3] or time- intensive manipulation with atomic force microscopy (AFM) [4]. Taking advantage of the versatility of plasmonic nanostructures in optical trapping/tweezing [7–14], simultaneous assembling and coupling with a dedicated plasmonic tweezer-nanoantenna has opened the opportunities of exploiting this platform as an on-chip, scalable and compact system for realizing quantum technologies. Furthermore, in such plasmonic trapping systems, utilization of the plasmonic-loss-induced temperature gradient in a colloidal system through electro-thermo-plasmonic (ETP) flow [15] and negative thermophoresis [16–18] has been demonstrated to provide an extra benefit in precise maneuvering and trapping of nano emitters of size as small as 10 nm [9,19].

However, along with deterministic on-chip integration of quantum emitters, efficient collection and routing of emitted single photon is also necessary to direct application in quantum information processing [20]. Some of the prior approaches on building chip-compatible single photon emitters involved fabrication of an embedded nano emitter adjacent to low-loss photonic substrate/waveguide to let the SPP coupled fluorescence out-couple to guided modes in the dielectric [21–23]. Such approaches involve refractive optics based free space excitation lacking the flexibility of remote operation and incompatible for integrated networks. Therefore, a compact

#477164 https://doi.org/10.1364/OE.477164
Journal © 2022 Received 5 Oct 2022; revised 3 Dec 2022; accepted 5 Dec 2022; published 16 Dec 2022

Optics EXPRESS

system with on-chip control of the functionalities like maneuvering, enhancement, and collection is desirable for implementation of integrated emitter-based quantum architecture.

Considering the shortcomings of previous approaches, here we are proposing a hybrid photonic waveguide-coupled plasmonic system configured to 'trap, enhance and guide'. Our proposed hybrid system device aims to achieve quick and high-precision trapping of nanoparticles (nano-emitters) and emission rate enhancement within the same structure with the on-chip operation flexibility. While the unique features of plasmonic system in nano focusing and field localization supports the main functionalities like long-range transport (ETP flow [15,24]), short-range trapping (optical force [25,26] and negative thermophoretic force), and emitter enhancement (Purcell effect [6]), a low loss dielectric waveguide beneath supports on-chip excitation and collection via evanescent coupling of the propagating signal. However, in forming a hybrid system, the effective coupling between plasmonic and photonic system must be ensured which depends on the effective mode index matching [27–29].To minimize probable scattering loss induced mode mismatch during excitation and collection by a waveguide, in our design we chose to work with a tapered plasmonic waveguide of metal-insulator-metal (MIM) configuration which has been extensively studied for adiabatic mode conversion feature [30,31] and it is placed and centered on top of Silicon waveguide, as shown in Fig. 1. To enable on-chip compatibility with existing CMOS technologies, our device design considered a silicon-on-insulator (SOI) waveguide. The Si waveguide transparency cutoff being around 1.1 µm, the system supports many popular colloidal quantum emitters [22,32–34] operating at room temperature and with broadband emission spectrums encompassing communication wavelength.

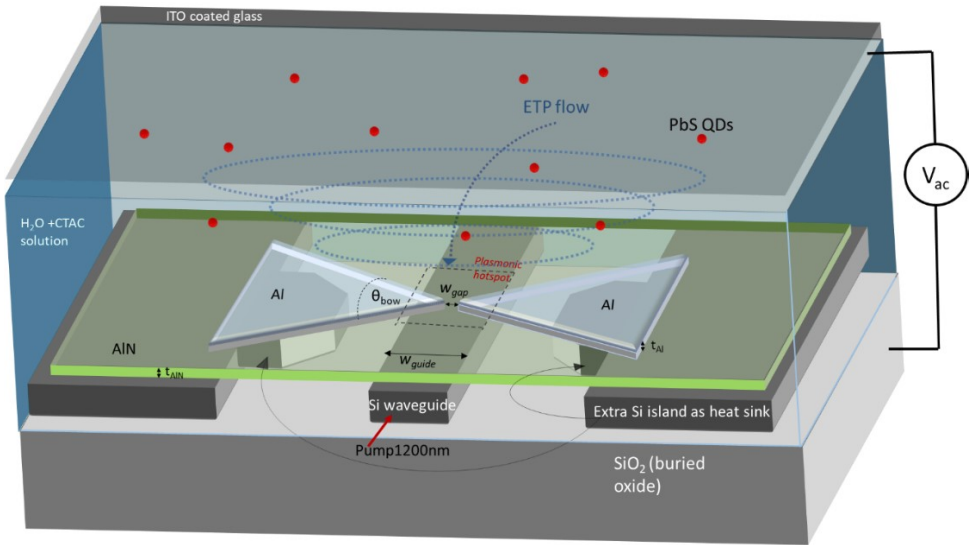

Fig. 1. Proposed device schematic. Transparency has been added to the layers for visual understanding.

2. Method

Scheme wise, our system considers achieving the goal of 'trap-enhance-guide' in a sequence of operations. First step is to enable sufficient trapping potential to capture a nano quantum dot with a diameter of approximately 10 nm. This is accomplished with pump light, polarized parallel to the surface, being input into the system through Si waveguide to excite the gap plasmon via evanescent coupling. The excited field hotspot at the tips of bowtie, and the induced local

Optics EXPRESS

temperature gradient from absorption, is then used to execute trapping of colloidal quantum dots with optical and attractive thermophoretic force along with ETP flow. Once trapping is ensured at the smallest MIM gap region, the structure aims to support large Purcell enhancement to the trapped emitter by coupling emission to plasmonic modes. Lastly, with the efficient energy transitions from the SPP mode to low loss waveguide mode, the emission couples into the dielectric waveguide to be collected for subsequent routing and processing on-chip. For this mode of operation, emitter can be 'printed' to the device and the system detached from microfluidic medium. As such, it will not require waveguide excitation for trapping, only for excitation of the emitter.

Towards the goal of implementing our proposed compact device, in this report we have assessed the feasibility of the scheme by evaluating the basic performance metrics considered for 'trap, enhance and guide' functions, these are- i. Attainable particle velocity with ETP flow for long range transport; ii. Trapping potential at hotspot location from conjugate forces (optical and thermophoretic forces); iii. Purcell enhancement factor at the trapping location; iv. Collection efficiency through dielectric Si waveguide. The analysis has been carried out by numerical simulation via finite element method in COMSOL Multiphysics. The following sections includes the simulation details and findings from the analysis which verifies and predicts the performance of our proposed scheme.

3. Results and discussion

For the evaluation of the performance metrics respective to the target functionalities discussed above, we set up a three-dimensional (3D) model of our designed structure and performed a modal analysis with Wave Optics module to find the suitable guided mode for the launched excitation. The evolution of mode profile with changing MIM gap along the propagation ultimately results into field confinement at the smallest gap region (see Supplement 1 section S1, Fig. S1). Following this, the schemes involving ETP flow and trapping mode operation are evaluated with a Wave Optics and Heat Transfer coupled Multiphysics model. The evaluation of Purcell enhancement and waveguide collection efficiency has been performed in a separate COMSOL model using a point dipole source in Wave optics module only. The values of structure dimensions used in the simulation are provided in Table S1 of Supplement 1. The detailed procedures and results of the performance metrics are discussed below according to the execution order of the overall scheme.

I. Calculation of thermal gradient induced rapid transport velocity via ETP Flow

The optical energy coupled into the MIM plasmonic waveguide experiences ohmic loss within and raises the temperature of the metal and surrounding fluid. As for the choice of material as metal and buffer layer (layer separating metal and top of planarized Si and SiO_2) to be used in our proposed device, we have singled out Aluminum thin films and Aluminum Nitride (AlN) respectively. In case of AlN, we have considered its suitability in reducing refractive index mismatch at the Si-metal-water interface as well as its high thermal conductivity which plays an important role in thermal management during the colloidal trapping function with plasmon excitation. In the simulation model for most of the device materials, e.g. Al, Si, SiO_2 and water, bulk optical and thermal property has been assumed as per the general database [35–38], except for the thermal conductivity of AlN thin film ($\kappa_{AlN} = 80$ W/m-K) [39].

To estimate the temperature rise, we carried out a 3D Multiphysics simulation incorporating Wave-optics and Heat-Transfer modules in COMSOL. Considering 20.15°C as the initial temperature as for room temperature operation and injection of 10 mW of 1200 nm light through the side port, initially the steady-state temperature rise has been found to be more than 100°C at the plasmonic hotspot (see Supplement 1 section S2, Fig. S2). Although the maximum temperature is still well below the melting point of Al (660°C), such high temperature rise can

Optics EXPRESS

cause natural convection in the fluid medium and hence is not recommended for the control of fluidic transport. Utilizing the high thermal conductivity of Si, we have considered an additional heat dissipation path in the design by adding an extra layer of Si below the metal films at non-interfering distance of at least 150 nm from the central Si WG, to mitigate rapid temperature rise of overall system (see Fig. 1). With this approach, the temperature rise has been reduced to a maximum of about 60°C which is sufficient to enable transport and trapping without the risk of boiling or other non-idealities, see Fig. 2(Left). While this temperature is manageable for the device, a lower rise of ~20-30°C is desired. This can be accomplished through additional optimization of the structure to provide more efficient thermal dissipation as well as reducing the required pump power.

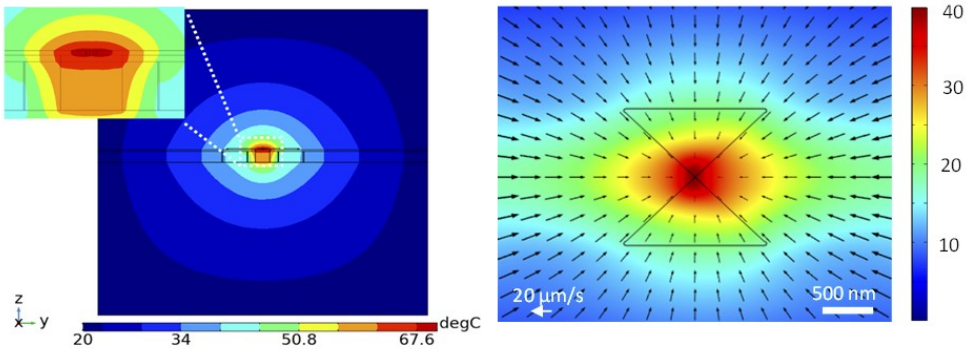

Fig. 2. (Left) Cross-sectional view of plasmon excitation induced temperature gradient around local hotspot. (Right) Temperature rise from initial room temperature and velocity of ETP flow induced under the application of an AC field to generate rapid transport to the hotspot. This is shown as top view.

The next step is to ensure rapid transport of emitters to the trapping site. Here, we utilize thermal gradient induced by Ohmic loss to produce a variation in the permittivity and electrical conductivity of the fluid, finally creating local net charge density. Under the application of an AC electric field, the induced charges respond to the external electric field and non-zero body force is expressed in:

$$f_{ET} = \rho_e E - \tfrac{1}{2}|E|^2 \nabla \varepsilon_m \tag{1}$$

After perturbative expansion in the limit of small temperature gradient, the force density is expressed as [40]:

$$f_{ET} = \tfrac{1}{2} Re\left\{\frac{\varepsilon(\alpha-\beta)(\nabla T.E)E^*}{\sigma+i\omega\varepsilon} + \tfrac{1}{2}\varepsilon\alpha|E|^2\nabla T\right\} \tag{2}$$

where $\alpha = {}^1/_{\varepsilon}\frac{d\varepsilon}{dT}$ and $\beta = {}^1/_{\sigma}\frac{d\sigma}{dT}$. ε stands for permittivity, σ stands for conductivity and ω is AC frequency. This net body force drives the fluid motion along the gradient of the temperature profile [15,40], which is called ETP flow. ETP flow transports particles to the region of high temperature rapidly which is the plasmonic thermal hotspot in this context. It is worth mentioning here that this electrothermal flow has a long working range and can access particles within several hundreds of micron range. Utilizing ETP flow can ensure fast transport of quantum emitters and the ability to work with low emitter concentration.

The AC electric field distribution used in the ETP flow body force density term in Eq. (2) is obtained by solving the Laplace's equation. By using the results of the temperature profile from the thermal simulation and AC electric field value from Laplace's equation, the Navier-Stokes equation is solved to obtain the velocity distribution due to the ETP flow. The force density term in the Navier-Stoke's equation is represented by the ETP flow body force term defined in Eq. (2)

Optics EXPRESS

(see Supplement 1 section S3 for computational details). For an AC electric field strength of 83 kV/m and frequency of 10 kHz, the radial ETP force is found to generate speeds on the order of 20 µm/s directed towards the hotspot, see Fig. 2(Right). This provides sufficient velocity to enable rapid transport of suspended emitters to the hotspot within seconds.

II. Estimation of trapping potential with conjugate forces

While the ETP flow generates rapid transit of the particle, it cannot provide stable and accurate trapping. To achieve the accurate positioning of a single emitter, we make use of a combination of optical gradient forces and negative thermophoretic forces. Theoretically, the strong optical confinement within the hotspot region generates large field gradients in the adjacent fluidic environment. When a particle is placed within this strongly non-uniform field, it experiences a net force pulling it towards the region of high field – called the optical gradient force [26] and in the quasi-static limit, it is expressed by-

$$F_{grad} = \frac{1}{2}\alpha\nabla E^2 \propto a^3\nabla E^2 \tag{3}$$

where α is the polarizability of the particle and a is the particle radius. We note that the scattering force, $F_{scat} \propto a^6E^2$ is negligible in our case due to the size of our emitter (radius ~5 nm).

In addition, we consider making use of the thermal gradient to induce an attractive negative thermophoretic force that works synergistically with the optical gradient force to increase trap stability for single emitters regardless of size. Generating the negative thermophoretic force directed towards the hotspot region will be achieved by introducing a cationic surfactant Cetyltrimethylammonium chloride (CTAC) to tune the permittivity of the electrical double layer surrounding the emitter. The equation, for the thermophoretic force is expressed as [18]:

$$F_{therm} = -K_BTS_T\nabla T \tag{4}$$

where K_B is the Boltzmann constant, S_T is the Soret coefficient, and T is the temperature (see Supplement 1 section S4 for computational details). Once the ETP flow of the fluid rapidly brings suspended emitters near the hotspot, the optical gradient force in the plasmonic cavity starts to exert trapping force onto the nanoparticle. However, due to the extremely tiny size of the target particles, like QDs (~10 nm in diameter), the Brownian motion of QDs is intense and increases the probability for QDs escaping from the cavity, even if the cavity has captured them. The negative thermophoresis, nevertheless, enhances the trapping stability by bringing in an additional attractive force into the system.

As target component, we have considered colloidal PbS QDs which are commercially available with room temperature emission near the telecom wavelength range and hence, appropriate with our proposed application [41]. In the simulation, the PbS QD is modeled as a sphere of 10 nm diameter with refractive index of 2.5 and thermal conductivity κ = 1.75 W/m-K [42,43]. Water being an excellent polar liquid and heat dissipater has been considered as submerging medium. For a particle trapped by a highly localized electric field, the traditional approach of calculating the induced optical force is to use Maxwell stress tensor (MST) which denotes the time averaged force density. As COMSOL wave-optics module has built-in MST solver, by integrating the tensor components over the target particle's surface area, the optical force components along Cartesian axes have been evaluated. Next, to assess the stability of the trap, the potential energy in integration form, $U(r) = -\int_{\infty}^{r} F(r') \cdot dr'$ has been used to calculate the potential energy experienced by the particle at varying distances, where r and r′ are position vector variables of the particle. On the other hand, by using the temperature profile obtained through thermal simulation, the negative thermophoretic force has been estimated using the Eq. (4). In both cases, the particle position has been varied along the horizontal XY plane near the hotspot zone.

Optics EXPRESS

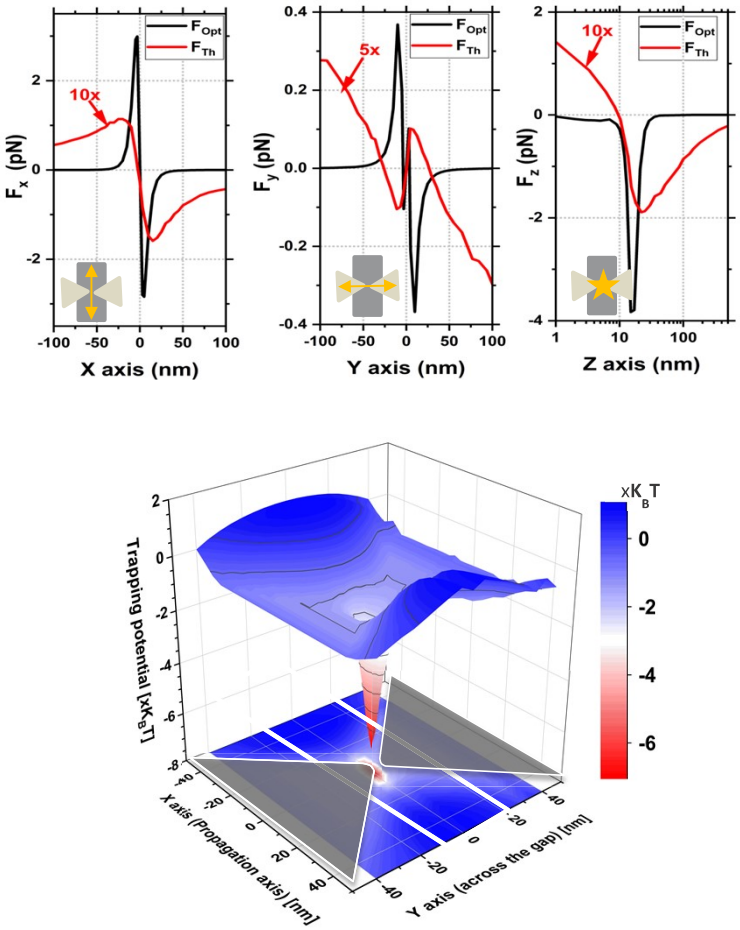

Fig. 3. (Top panel) Contribution of optical force and thermophoretic force along different directions with respect to the simulation model for a 10 nm QD. The thermophoretic forces have been magnified to fit the scale of optical force shown in the same plot and the scaling parameter is mentioned in the respective plot windows. (Bottom panel) Overall trapping potential at the hotspot calculated from conjugate trapping force acting on 10 nm PbS QD.

As shown in Fig. 3 (top panel) strong trapping forces are felt in the hotspot region due to the simultaneous localization of thermal and electric fields. Although the thermophoretic forces appear small near the hotspot, it provides stronger gradients on the micron scale, bridging the gap between the macroscopic ETP flow and nanoscopic gradient force. As a result, the conjugation of forces enables a trap depth of ~8 K_BT (~2 K_BT for negative thermophoretic force and ~6 K_BT for optical gradient force) (see Fig. 3) where T is taken as the local temperature in the trapping region and K_B is the Boltzmann constant. While in literature, a potential of 10 K_BT is often recommended for stable trapping with conventional method with direct irradiation [11], it has been experimentally observed that with gap-plasmon excitation, nanoparticle trapping of comparable size is achievable even for potentials well below this threshold [7,44]. From theoretical perspective, one of the sufficient conditions for stable trapping is to have longer diffusion or escape time (τ_{escape}) of a trapped particle from the potential well due to Brownian motion compared to the trapping time and this is expressed with the Boltzmann factor, $exp\left(-\frac{\Delta U}{K_B T}\right) \ll 1$ where ΔU refers to the well depth [25]. Our estimated potential fulfills this condition sufficiently assuring

Optics EXPRESS

the chances of target object escaping the trap would still be considerably low and can be redeemed by slightly compromising with the re-trapping time.

III. Emission enhancement & collection

For an emitter located at the tips where the field enhancement is the highest, the predominant modes available to the emitter are high k (momentum) plasmonic modes in the MIM waveguide structure which ultimately helps to enhance radiative decay rate leading to a high Purcell factor. For simplicity, a quantum emitter can be considered as a two level atomic system interacting with its electromagnetic environment and the interaction with a single-mode can be described in terms of the dipole moment [45,46]. Hence, the quantum emitter is modeled as a point dipole for the simulation study. To estimate the spatial Purcell enhancement, the model dipole emitter's position was swept through the hotspot region in a 3D FEM simulation with wave-optics module, and the average power crossing the surface of a sphere of 1 nm radius centered on the dipole was computed [2]. By comparing it to the outward power for the dipole-sphere placed in air, we quantified the Purcell enhancement factor $\left(= \frac{P_{out}\text{ in hybrid structure}}{P_{out}\text{ in air}}\right)$[47]. To account for orientation error of the emitter, Purcell factors for a dipole oriented along the x, y, and z axes were noted and averaged at each position. As shown in Fig. 4(Left), a strong enhancement of 500 - 4,000 depending on the location is found, averaging 2,000 in the hotspot.

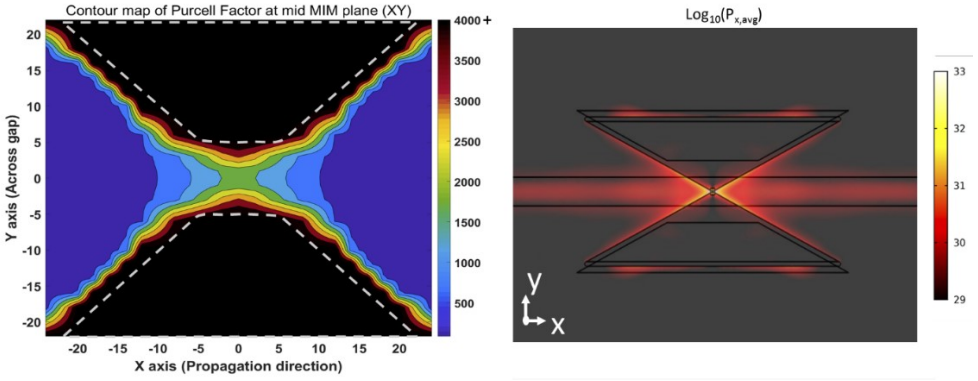

Fig. 4. (Left) Orientation averaged Purcell Factor of a dipole emitter near the hotspot (trapping region). The dashed white boundary refers to the metal area. (Right) Logarithmic plot of the power flow from dipole emitter along x direction, parallel to waveguide propagation. The brighter zone refers to increasing intensity.

To estimate the collection efficiency, the dipole emitter is placed in the middle of gap region. By taking the ratio of outgoing power through waveguide cross-sections at two port ends to total power radiated from the emitter dipole, bidirectional collection efficiency is found to be 10%. The routing of power flow through the waveguide has been shown by plotting logarithmic power density in Fig. 4(Right). The emission could be made unidirectional by including a Bragg reflector or ring-resonator on one end of the device that is designed to achieve high reflectivity at the output wavelength of the emitter while transmitting the pump. Through the optimization of the hotspot region and the plasmonic-to-photonic coupling, there are further scopes to improve the directionality and collection efficiency.

4. Conclusion

In summary, we have evaluated the preliminary performance outcomes of our proposed scheme involving simultaneous trapping, emission enhancement and guiding, executed with same

Optics EXPRESS

waveguide coupled hybrid plasmonic structure. With numerical simulation, we have analyzed the performance of the system in the context of the device features, e.g., long range transport, trapping, enhancement, and on-chip collection efficiency. Overall, the proposed device estimates rapid (within seconds), long-range (mm-scale), accurate (<10 nm), and stable (~8 K_BT) trapping of single particles (d ~ 10 nm), alongside strong Purcell enhancement (PF ~ 1,000), with excitation/collection through an on-chip waveguide. Besides the multifunctional features of the proposed system discussed here, there is also a practical scope for additional testing and verification feature by tuning the applied field (AC/DC) used for ETP. By appropriately switching external field nature between AC/DC during ETP flow operation, trapped particles can either be permanently printed or released from the trapping location [15]. This feature can provide extra flexibility of testing and verifying the fluorescence lifetime quality and even $g^{(2)}$ correlation measurement before permanently 'printing' the emitter to device. Therefore, once realized, our proposed scheme will contribute to developing an on-chip integrated platform of non-classical light-based applications with low-cost, scalable, and deterministic route to assemble and interact with single and multiple quantum emitters that is so far missing.

Funding. Commonwealth Cyber Initiative (CCI); Virginia Commonwealth University 2021 Presidential Research Quest Fund; National Science Foundation (NSF ECCS-1933109).

Acknowledgments. The work was partially supported by Commonwealth Cyber Initiative (CCI) program and Virginia Commonwealth University 2021 Presidential Research Quest Fund. C.H. and J.C.N. acknowledge support from National Science Foundation (NSF ECCS-1933109).

Disclosures. The authors declare no conflicts of interest.

Data availability. Some of the parametric data used in the COMSOL model to obtain the results presented in this paper are available in Table S1 of Supplement 1. Additional information may be obtained from the authors upon reasonable request.

Supplemental document. See Supplement 1 for supporting content.

References

1. S. I. Bozhevolnyi and J. B. Khurgin, "The case for quantum plasmonics," *Nature Photonics*, vol. 11, no. 7. Nature Publishing Group, pp. 398–400, 30-Jun-2017.
2. G. M. Akselrod, C. Argyropoulos, T. Hoang, C. Ciraci, C. Fang, J. Huang, D. R. Smith, and M. H. Mikkelsen, "Probing the mechanisms of large Purcell enhancement in plasmonic nanoantennas," Nat. Photonics **8**(11), 835–840 (2014).
3. S. I. Bogdanov, O. Makarova, X. Xu, Z. O. Martin, A. S. Lagutchev, M. Olinde, D. Shah, S. N. Chowdhury, A. R. Gabidullin, I. A. Ryzhikov, I. A. Rodionov, A. V. Kildishev, S. I. Bozhevolnyi, A. Boltasseva, V. M. Shalaev, and J. B. Khurgin, "Ultrafast quantum photonics enabled by coupling plasmonic nanocavities to strongly radiative antennas," Optica **7**(5), 463 (2020).
4. S. K. H. Andersen, S. I. Bogdanov, O. Makarova, Y. Xuan, M. Y. Shalaginov, A. Boltasseva, S. I. Bozhevolnyi, and V. M. Shalaev, "Hybrid Plasmonic Bullseye Antennas for Efficient Photon Collection," ACS Photonics **5**(3), 692–698 (2018).
5. E. M. Purcell, H. C. Torrey, and R. V. Pound, "Resonance absorption by nuclear magnetic moments in a solid [7]," Physical Review, vol. 69, no. 1–2. American Physical Society, pp. 37–38, 01-Jan-1946.
6. E. M. Purcell, "Spontaneous Emission Probabilities at Radio Frequencies," (Springer, 1995, p. 839).
7. R. A. Jensen, I. Huang, O. Chen, J.T. Choy, T.S. Bischof, M. Lončar, and M. G. Bawendi, "Optical Trapping and Two-Photon Excitation of Colloidal Quantum Dots Using Bowtie Apertures," ACS Photonics **3**(3), 423–427 (2016).
8. Z.-S. Li, T.-W. Lu, T.-W. Lu, P.-R. Huang, P.-T. Lee, and P.-T. Lee, "Efficient nano-tweezers via a silver plasmonic bowtie notch with curved grooves," Photon. Res. **9**(3), 281–288 (2021).
9. Q. Jiang, P. Roy, J.-B. Claude, and J. Me Wenger, "Single Photon Source from a Nanoantenna-Trapped Single Quantum Dot," Nano Lett. **21**(16), 7030–7036 (2021).
10. P. Zhang, G. Song, and L. Yu, "Optical trapping of single quantum dots for cavity quantum electrodynamics," Photon. Res. **6**(3), 182 (2018).
11. P. T. Lin, H. Y. Chu, T. W. Lu, and P. T. Lee, "Trapping particles using waveguide-coupled gold bowtie plasmonic tweezers," Lab Chip **14**(24), 4647–4652 (2014).
12. W. Zhang, L. Huang, C. Santschi, and O. J. F. Martin, "Trapping and Sensing 10 nm Metal Nanoparticles Using Plasmonic Dipole Antennas," Nano Lett. **10**(3), 1006–1011 (2010).
13. P. M. Bendix, L. Jauffred, K. Norregaard, and L. B. Oddershede, "Optical trapping of nanoparticles and quantum dots," *IEEE J. Sel. Top. Quantum Electron.* 20(3), (2014).

Optics EXPRESS

14. Y. Zhang, C. Min, X. Dou, X. Wang, H. P. Urbach, M.G. Somekh, and X. Yuan,"Plasmonic tweezers: for nanoscale optical trapping and beyond," Light: Science and Applications, vol. 10(1). Springer Nature, pp. 2047–7538, 01-Dec-2021.
15. J. C. Ndukaife, A. V. Kildishev, A. G. A. Nnanna, V. M. Shalaev, S. T. Wereley, and A. Boltasseva, "Long-range and rapid transport of individual nano-objects by a hybrid electrothermoplasmonic nanotweezer," Nat. Nanotechnol. **11**(1), 53–59 (2016).
16. . E. H. Hill, J. Li, L. Lin, Y. Liu, and Y. Zheng, "Opto-Thermophoretic Attraction, Trapping, and Dynamic Manipulation of Lipid Vesicles," Langmuir **34**(44), 13252–13262 (2018).
17. L. Lin, J. Zhang, X. Peng, Z. Wu, A. C. H. Coughlan, Z. Mao, M. A. Bevan, and Y. Zheng, "Opto-thermophoretic assembly of colloidal matter," *Sci. Adv.* 3(9), (2017).
18. L. Lin, M. Wang, X. Peng, E. N. Lissek, Z. Mao, L. Scarabelli, E. Adkins, S. Coskun, H. E. Unalan, B. A. Korgel, L. M. Liz-Marzán, E. Florin, and Y. Zheng, "Opto-thermoelectric nanotweezers," Nat. Photonics **12**(4), 195–201 (2018).
19. C. Hong, S. Yang, I. I. Kravchenko, and J. C. Ndukaife, "Electrothermoplasmonic Trapping and Dynamic Manipulation of Single Colloidal Nanodiamond," Nano Lett. **21**(12), 4921–4927 (2021).
20. P. Lodahl, S. Mahmoodian, and S. Stobbe, "Interfacing single photons and single quantum dots with photonic nanostructures," Reviews of Modern Physics 87(2). American Physical Society, pp. 347–400, 11-May-2015.
21. C. C. Chiang, S. I. Bogdanov, O. Makarova, X. Xu, S. Saha, D. Shah, Z. O. Martin, D. Wang, A. S. Lagutchev, A. V. Kildishev, A. Boltasseva, and V. M. Shalaev, "Chip-Compatible Quantum Plasmonic Launcher," Adv. Optical Mater. **8**(20), 2000889 (2020).
22. L. Elsinger, R. Gourgues, I. E. Zadeh, J. Maes, A. Guardiani, G. Bulgarini, S. F. Pereira, S. N. Dorenbos, V. Zwiller, Z. Hens, and D. V. Thourhout, "Integration of Colloidal PbS/CdS Quantum Dots with Plasmonic Antennas and Superconducting Detectors on a Silicon Nitride Photonic Platform," Nano Lett. **19**(8), 5452–5458 (2019).
23. F. Böhm, N. Nikolay, C. Pyrlik, J. Schlegel, A. Thies, A. Wicht, G. Tränkle, and O. Benson, "On-chip integration of single solid-state quantum emitters with a SiO2 photonic platform," New J. Phys. **21**(4), 045007 (2019).
24. C. Hong, S. Yang, and J. C. Ndukaife, "Stand-off trapping and manipulation of sub-10 nm objects and biomolecules using opto-thermo-electrohydrodynamic tweezers," Nat. Nanotechnol. **15**(11), 908–913 (2020).
25. A. Ashkin, J. M. Dziedzic, J. E. Bjorkholm, and S. Chu, "Observation of a single-beam gradient force optical trap for dielectric particles," in Optical Angular Momentum, vol. 11, no. 5, CRC Press, 2016 196–198.
26. K. C. Neuman and S. M. Block, "Optical trapping," Rev. Sci. Instrum. **75**(9), 2787–2809 (2004).
27. F. B. Arango, A. Kwadrin, and A. Femius Koenderink, "Plasmonic Antennas Hybridized with Dielectric Waveguides," ACS Nano **6**(11), 10156–10167 (2012).
28. N. A. Güsken, M. P. Nielsen, N. B. Nguyen, S. A. Maier, and R. F. Oulton, "Nanofocusing in SOI-based hybrid plasmonic metal slot waveguides," Opt. Express **26**(23), 30634 (2018).
29. M. Sojib, D. Fomra, V. Avrutin, Ü. Özgür, and N. Kinsey, "Optimizing epsilon-near-zero based plasmon assisted modulators through surface-to-volume ratio," Opt. Express **30**(11), 19781 (2022).
30. M. I. Stockman, "Nanofocusing of Optical Energy in Tapered Plasmonic Waveguides," Phys. Rev. Lett. **93**(13), 137404 (2004).
31. H. Choo, M. Kim, M. Staffaroni, T. J. Keok, J. Bokor, S. Cabrini, P. J. Schuck, M. C. Wu, and E. Yablonovitch, "Nanofocusing in a metal–insulator–metal gap plasmon waveguide with a three-dimensional linear taper," Nat. Photonics **6**(12), 838–844 (2012).
32. J. C. Weeber, K. Hammani, G. Colas-des-Francs, A. Bouhelier, J. Arocas, A. Kumar, F. Eloi, S. Buil, X. Quélin, J. Hermier, M. Nasilowski, and B. Dubertret, "Colloidal Quantum Dot Integrated Light Sources for Plasmon Mediated Photonic Waveguide Excitation," ACS Photonics **3**(5), 844–852 (2016).
33. M. Humer, R. Guider, T. Fromherz, and W. Jantsch, "Integration, photostability and spontaneous emission rate enhancement of colloidal PbS nanocrystals for Si-based photonics at telecom wavelengths," Opt. Express **21**(16), 18680–18688 (2013).
34. S. Tamariz, G. Callsen, J. Stachurski, K. Shojiki, R. Butté, and N. Grandjean, "Toward Bright and Pure Single Photon Emitters at 300 K Based on GaN Quantum Dots on Silicon," ACS Photonics **7**(6), 1515–1522 (2020).
35. K. M. McPeak, S. V. Jayanti, S. J. P. Kress, S. Meyer, S. Iotti, A. Rossinelli, and D. J. Norris, "Plasmonic films can easily be better: Rules and recipes," ACS Photonics **2**(3), 326–333 (2015).
36. M. A. Green and M. J. Keevers, "Optical properties of intrinsic silicon at 300 K," Prog. Photovolt: Res. Appl. **3**(3), 189–192 (1995).
37. I. H. Malitson, "Interspecimen Comparison of the Refractive Index of Fused Silica*,†," J. Opt. Soc. Am. **55**(10), 1205–1209 (1965).
38. M. L. V. Ramires, C. A. Nieto Castro, Y. Nagasaka, A. Nagashima, M. J. Assael, and W. A. Wakeham, "Standard Reference Data for the Thermal Conductivity of Water," J. Phys. Chem. Ref. Data **24**(3), 1377–1381 (1995).
39. K. Ait Aissa, N. Semmar, D. De Sousa Meneses, L. Le Brizoual, M. Gaillard, A. Petit, P-Y. Jouan, C. Boulmer-Leborgne, and M. A. Djouadi, "Thermal conductivity measurement of AlN films by fast photothermal method," in *Journal of Physics: Conference Series*, 2012, vol. 395, no. 1, p. 012089.
40. A. Ramos, H. Morgan, N. G. Green, and A. Castellanos, "Ac electrokinetics: a review of forces in microelectrode structures," J. Phys. D: Appl. Phys. **31**(18), 2338–2353 (1998).

Optics EXPRESS

41. J. J. Peterson and T. D. Krauss, "Fluorescence spectroscopy of single lead sulfide quantum dots," Nano Lett. **6**(3), 510–514 (2006).
42. T. Kyprianidou-Leodidou, W. Caseri, and U. W. Suter, "Size Variation of PbS Particles in High-Refractive-Index Nanocomposites," J. Phys. Chem. **98**, 8992–8997 (1994).
43. H. Zhang, H. Wang, H. Zhu, H. Li, T. Su, S. Li, M. Hu, and H. Fan, "Hydrothermal synthesis and thermoelectric properties of PbS," Mater. Sci. Poland **34**(4), 754–759 (2016).
44. Y. Tsuboi, T. Shoji, N. Kitamura, M. Takase, K. Murakoshi, Y. Mizumoto, and H. Ishihara, "Optical trapping of quantum dots based on gap-mode-excitation of localized surface plasmon," J. Phys. Chem. Lett. **1**(15), 2327–2333 (2010).
45. H. Groß, J. M. Hamm, T. Tufarelli, O. Hess, and B. Hecht, "Near-field strong coupling of single quantum dots," *Sci. Adv.* 4(3), (2018).
46. S. Hesabi, D. Afshar, and M. G. A. Paris, "Non-Markovian evolution of a two-level system interacting with a fluctuating classical field via dipole interaction," Opt. Commun. **437**, 377–381 (2019).
47. A. E. Krasnok, A. P. Slobozhanyuk, C. R. Simovski, S. A. Tretyakov, A. N. Poddubny, A. E. Miroshnichenko, Y. S. Kivshar, and P. A. Belov, "An antenna model for the Purcell effect," Sci. Rep. **5**(1), 12956–16 (2015).